# TRAJECTORY OPTIMIZATION OF A SMALL AIRSHIP IN A MOVING FLUID

Charles Blouin[1], Eric Lanteigne[1] and Wail Gueaieb[2]
[1]*Department of Mechanical Engineering, University of Ottawa, Ottawa, ON, Canada*
*E-mail: cblou045@uottawa.ca; eric.lanteigne@uottawa.ca*
[2]*School of Electrical Engineering and Computer Science, University of Ottawa, Ottawa, ON, Canada*
*E-mail: wgueaieb@uottawa.ca*

Received July 2015, Accepted November 2015
No. 15-CSME-71, E.I.C. Accession 3846

## ABSTRACT
Airships offer a low-cost alternative to heavier-than-air vehicles for long endurance applications in surveillance and transport. Although manoeuvring an under-actuated vehicle in a real environment while taking into account the obstacles, the dynamical model, the wind, and the energy consumption has been studied extensively, planning complex manoeuvres in constrained environments remains an active research area. This paper examines the use of optimal control for the trajectory planning of a small airship. The dynamic model of the vehicle and the experimental characterization of the drag coefficient are presented first, followed by the description of the trajectory planning problem formulated as an optimal control problem. Two trajectories are then solved using a pseudo-spectral solver to demonstrate that an optimal control approach can be used to generate complex and realistic manoeuvres.

**Keywords:** optimal control; airships; trajectory optimization; pseudo-spectral method.

# OPTIMISATION DE LA TRAJECTOIRE D'UN PETIT DIRIGEABLE DANS UN FLUIDE EN MOUVEMENT

## RÉSUMÉ
Les dirigeables offrent une alternative à bas coût pour les vols de longue endurance pour la surveillance et le transport. Manoeuvrer dans un environnent réel, prenant en compte les obstacles, le modèle dynamique du véhicule, le vent, et de la consommation d'énergie est un problème complexe. Ce document présentera le modèle dynamique d'un petit dirigeable et sa caractérisation dynamique expérimentale, suivie par la description du problème d'optimisation de trajectoire présenté comme un problème de contrôle optimal. Le problème sera ensuite résolu en utilisant une méthode pseudo-spectrale, implémentée dans le logiciel PSOPT. Ce papier démontre qu'une approche de contrôle optimale peut être utilisée pour générer des trajectoires complexes et très réalistes pour un petit dirigeable.

**Mots-clés :** contrôle optimal; dirigeable; trajectoire optimale; méthode pseudo-spectrale.

## 1. INTRODUCTION

Airships have seen a renewed interest since the beginning of the millennium. Their inherent safety, long range, endurance, and flight time makes them ideal as surveillance and monitoring platforms [1]. As an example, the United States army had a monitoring program involving an airship stationed at high altitude and a prototype was built in 2011 [2]. The vehicle was designed to provide 16kW to the surveillance payload, have an operating range of 2000 miles, and stay in the air for 21 days. Since airships are under-actuated and underpowered, there is a need to precisely control the airship during certain critical flight regimes such as at take-off, landing, or during close proximity operations in urban areas.

The trajectory or path planning problem is typically described by the optimization of a cost function, which is generally an integral over the path. This integral is typically a function of the local wind vector, flight time, the path local orientation and vehicle's properties. To explore possible paths, one approach is to discretize the search space in nodes and segments connecting those nodes [3]. A weight is assigned to each segment and an algorithm such as A* or B* can be used to solve for the path [4]. Although fast, these methods are limited to long paths relative to the vehicle size, as they rarely take into account the dynamical model of the vehicle.

Numerous studies have shown that optimal control solvers are well suited for solving the path planning problem provided the dynamics of the vehicle are well known. Optimal control for trajectory optimization has historically been used in aerospace for the optimal ascent of rockets as it takes into account all the differential constraints of the model and the environment [5, 6]. More recently the method has also been applied to the path planning of aircraft [7]. Since analytical solutions are only possible in very simple and specific cases, numerical solutions are typically used. In this paper, optimal control is applied to the trajectory planning problem of a small airship. The cost function is minimized using the pseudo-spectral method for optimal control. Pseudo-spectral solvers were initially investigated for solutions to PDEs in fluid dynamics. For example, solutions to the well known 1D Burgers equation as well as the 3D Euler equations were obtained using these solvers [8].

The remainder of this paper is organized as follows: first, the dynamics of the vehicle are presented, followed by the kinematics and kinetic equations. Then, an experimental drag model is presented and two simulated paths obtained using optimal control are examined.

## 2. AIRSHIP MODEL

Airships are typically modelled using Newton's equations in a local coordinate frame fixed to the centre of volume (CV) of the vehicle. The small airship used in the simulation is shown in Fig. 1 and is based on the Microblimp from Plantraco with a custom helium envelop to increase lift. The airship is modelled as a six degrees of freedom rigid body in a viscous fluid, with experimentally determined values for rotational damping and drag.

The governing equations for an airship can be expressed as

$$\mathbf{M}\ddot{\mathbf{x}} = \mathbf{F_d}\dot{\mathbf{x}} + \mathbf{A}\dot{\mathbf{x}} + \mathbf{G} + \mathbf{PU} \tag{1}$$

where $\mathbf{M}$ is a $6\times6$ mass matrix, including the rotational inertial and the virtual masses, $\dot{\mathbf{x}} = [\mathbf{v} \mid \boldsymbol{\omega}]^T$ are the velocities of the vehicle, $\mathbf{F_d}\dot{\mathbf{x}}$ is due to the offset between the centre of axis and the centre of mass, $\mathbf{A}$ is the aerodynamic vector, $\mathbf{G}$ is the buoyancy vector, $\mathbf{P}$ is the propulsion matrix, and $\mathbf{u}$ is the control vector. The dynamic term $\mathbf{F_d}$ is a function of the angular rate of rotation and the mass matrix.

## 3. KINEMATIC EQUATIONS

The optimal control solver is independent of the method used to describe the vehicle pose, however, minimizing the number of states describing the pose simplifies the problem by reducing the size of the matrices

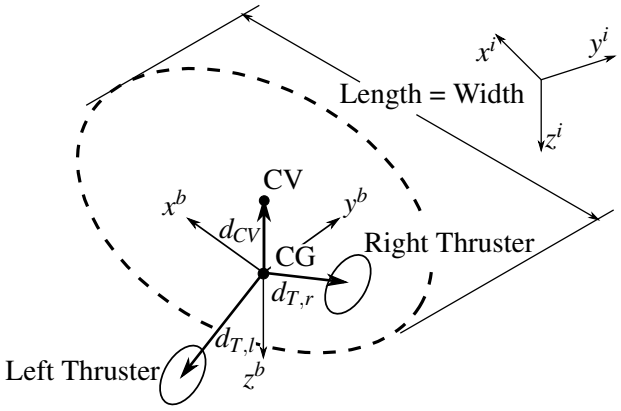


Fig. 1. Airship model.

and the memory used to solve the path. As a consequence, Euler angles were adopted as opposed to quaternions.

The airship is modelled as a rigid body with mass **m** and inertia **I**, with decoupled linear and rotational terms. Contrary to most literature on airship modelling, the equations of motion are written in the body reference frame around the Centre of Gravity (CG). This representation has the advantage of eliminating the transformation of the applied torque and forces from the inertial frame to the body frame.

The body reference frame is denoted with the superscript $b$ and the inertial reference frame denoted by the superscript $i$. The orientation of the vehicle is expressed using the roll ($\phi$), pitch ($\theta$), and yaw ($\psi$) convention. As such, the relation between the coordinates of the body reference frame to the fixed reference frame can be expressed as

$$\mathbf{S}^{b\to i}\mathbf{v}^b = \mathbf{v}^i \tag{2}$$

where the transformation matrix $\mathbf{S}^{b\to i}$ is given by

$$\mathbf{S}^{b\to i} = \begin{bmatrix} \cos\psi\cos\theta & -\sin\psi\cos\phi+\cos\psi\sin\theta\sin\phi & \sin\psi\sin\phi+\cos\psi\sin\theta\cos\phi \\ \sin\psi\cos\theta & \cos\psi\cos\phi+\sin\psi\sin\theta\sin\phi & -\cos\psi\sin\phi+\sin\psi\sin\theta\cos\phi \\ -\sin\theta & \cos\theta\sin\phi & \cos\theta\cos\phi \end{bmatrix} \tag{3}$$

and the velocity vector is given by

$$\mathbf{v} = [\dot{x}_x \quad \dot{x}_y \quad \dot{x}_z]^T \tag{4}$$

## 4. KINETIC EQUATIONS

The acceleration of the vehicle in the body reference frame is simplified to

$$\begin{bmatrix} \ddot{x}_x^b \\ \ddot{x}_y^b \\ \ddot{x}_z^b \end{bmatrix} = \begin{bmatrix} F_x^b/m_x \\ F_y^b/m_y \\ F_z^b/m_z \end{bmatrix} - \begin{bmatrix} p \\ q \\ r \end{bmatrix} \cdot \begin{bmatrix} \dot{x}_x^b \\ \dot{x}_y^b \\ \dot{x}_z^b \end{bmatrix} \tag{5}$$

where $m_x$, $m_y$ and $m_z$ are the virtual masses along the body axes, and the dot product between the angular velocity vector $\dot{\omega} = [p \quad q \quad r]^T$ in the body reference frame and the linear velocity in the body reference frame corresponds to forces due to the non-inertial frame of reference. The input forces $\mathbf{F}^b$ are modelled around the CG in the body reference frame. Those input forces are due to the buoyancy force, the gravity,

the aerodynamic drag and lift, as well as the thrust from the propellers. In Eq. (5), the term $\mathbf{F}^b$ is equal to the right hand side of (1).

$$\mathbf{F}^b = \mathbf{S}^{i\to b}\mathbf{B}^i + \mathbf{S}^{i\to b}\mathbf{G}^i + \mathbf{D}^b + \mathbf{T}^b \tag{6}$$

In the simulation, the vehicle is assumed to be neutrally buoyant, therefore the buoyancy force is canceled by the gravity force. The drag $\mathbf{D}^b$ is proportional to the relative vehicle velocity $\mathbf{v}_r^b = \mathbf{v}^b - \mathbf{S}^{i\to b}\mathbf{v}_w^i$ of the vehicle velocity in the body reference frame with respect to the wind velocity $\mathbf{v}_w$, and the vector of drag coefficients $\mathbf{C}(\phi,\theta,\psi,\mathbf{v}_w)$ depends on the angle of attack of the airship and the wind velocity.

$$\mathbf{D}^b = \mathbf{C}(\phi,\theta,\psi,\mathbf{v}_w)\mathbf{v}_r^b|\mathbf{v}_r^b| \tag{7}$$

The thrust vector $\mathbf{T}^b$ is the sum of the thrust from left and right thrusters $T_{\text{left}}$ and $T_{\text{right}}$.

$$\mathbf{T}^b = [T_{\text{left}} + T_{\text{right}} \quad 0 \quad 0]^T; \tag{8}$$

Similar to the input forces, the input moments $\mathbf{M}^b$ are modelled around the centre of gravity in the body reference frame. The moments acting on the vehicle include those due to the drag, the buoyancy, and the thrust forces.

$$\mathbf{M}^b = \mathbf{d}_{CV}\mathbf{S}^{i\to b}\mathbf{B}^i + \mathbf{d}_D\mathbf{D}^b + \mathbf{M}_T^b \tag{9}$$

where $\mathbf{d}_{CV}$ is the distance between the centre of gravity and the centre of volume, and $\mathbf{d}_D$ is the distance between the centre of gravity and the centre of drag. In the simulation, the centre of volume will be approximated to be at the same position as the centre of drag. The term

$$\mathbf{M}_T^b = \mathbf{d}_{T,l} \times [T_{\text{left}} \quad 0 \quad 0]^T + \mathbf{d}_{T,r} \times [T_{\text{right}} \quad 0 \quad 0]^T$$

is the sum of moments caused by the thrust forces from the thrusters.

The angular rate of change of the vehicle in the body frame is then given by

$$\dot{\omega} = \mathbf{I}^{-1}(\mathbf{M}^b - \omega \times \mathbf{I}\omega) \tag{10}$$

and the rate of change of the Euler angles can then be found from

$$\begin{bmatrix}\dot{\phi}\\ \dot{\theta}\\ \dot{\psi}\end{bmatrix} = \begin{bmatrix}1 & \sin\phi\tan\theta & \cos\phi\tan\theta\\ 0 & \cos\phi & -\sin\phi\\ 0 & \frac{\sin\phi}{\cos\theta} & \frac{\cos\phi}{\cos\theta}\end{bmatrix}\begin{bmatrix}p\\ q\\ r\end{bmatrix} \tag{11}$$

In summary, the state-space equations used in the optimal control solver are (2), (5), (10) and (11).

### 4.1. Drag Model

The rotational drag terms are often ignored for aircraft since, at high speeds, the aerodynamic forces from the control surface become relatively large. In the case of small airships, such as the one studied in this paper, the damping from fluid forces is significant and must be evaluated since the large mass of air displaced by the airship, relative to the mass of the airship itself, creates a virtual mass and inertia [9]. The rotational drag coefficient is often estimated by approximating the vehicle as a large cylinder, by using the potential flow assumption, or evaluated experimentally by placing a model in a wind tunnel [10]. The drag forces for the present model were found experimentally by capturing the position of a modified Microblimp with added ballast in free fall and fitting the resulting path to the following simplified equation of motion:

$$ma = F_g - F_d \tag{12}$$

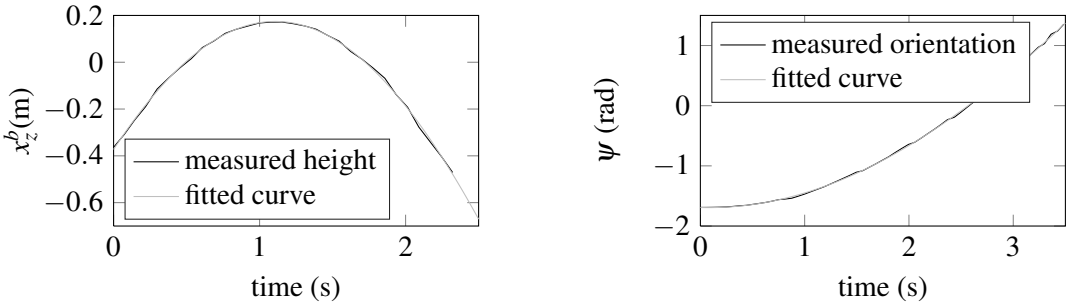


(a) Height as a function of time for the drop test in the forward-aft direction

(b) Orientation as a function of time during yaw characterization

Fig. 2. Characterization experiment of the airship.

where $m$ is the total mass of the vehicle, including the virtual mass from the air, $F_g$ is the gravity force, $F_d$ is the drag force, and $a$ is the acceleration vector. Each drag experiment experiment is performed in one dimension, so only the magnitude of the vector is considered. The drag force in the $z$ direction is

$$F_d = C_z(\dot{x}_z^b)^2 \tag{13}$$

The solution to (12) and (13) is

$$x_z^b(t) = \frac{m_{ez}\log\left(\cosh\frac{\sqrt{C_z}\sqrt{F_g}(c_1 m_{ez}+t)}{m_{ez}}\right)}{C_z} + c_2 \tag{14}$$

where parameter $C_z$ is the drag coefficient in the $z$ direction, $m_{ez}$ is the total mass of the airship and ballast, and $c_1$ and $c_2$ are related to the initial time and the absolute value of the initial altitude. Multiple drop tests were performed in the $x$ and $z$ directions to obtain the drag and the mass constants shown in Table 1. An example of two experimental paths in shown in Fig. 2. The mass obtained from the fitted curve includes the added mass from the displaced airflow. The results show that the added mass depends on the orientation of the airflow and varies between 30% of added mass to 110% of added mass for the modified Microblimp, depending on the orientation.

The characterization of the rotational damping followed the same procedure as the linear damping. The dynamic equation has the same form, but the velocity is replaced by the angular velocity $\omega$:

$$M_a = C_{rz}\dot{\phi}^2 \tag{15}$$

where $M_a$ is the applied torque and $C_r$ is the drag coefficient in rotation. The solution for the $z$ axis is then

$$\phi(t) = \frac{I_{ez}\log(\cosh\frac{\sqrt{C_{rz}}\sqrt{M_a}(d_1 I_{ez}+t)}{I_{ez}})}{C_{rz}} + d_2 \tag{16}$$

The solution for the $x$ and $y$ axes is the same, but the constants have different values due to the different geometry. The torque $M_a$ is applied by the two thrusters. The thrusters are set to 100% thrust and the airship is released. The pose of the airship is then recorded, and the unknown constants $C_{rz}$, $I_{ez}$, $d_1$, and $d_2$ are computed using curve fitting on the experimental data.

Table 1. Experimental value characterizing the airship.

| Variable | Description | Value | unit | 95 % conf. |
|---|---|---|---|---|
| $C_x$ | Horizontal linear drag coefficient | 0.046 | | $\pm 0.04$ |
| $C_z$ | Vertical linear drag coefficient | 0.11 | | $\pm 0.04$ |
| $m_{ex}$ | Experimental total mass in the $x$ axis | 0.077 | kg | $\pm 0.010$ |
| $m_{ez}$ | Experimental total mass in the $z$ axis | 0.117 | kg | $\pm 0.020$ |
| $m_b$ | Mass of the gondola, battery and balloon | 0.0357 | kg | $\pm 0.005$ |
| $m_g$ | Theoretical mass of the gas | 0.0258 | kg | $\pm 0.001$ |
| $m_b + m_g$ | Mass of the vehicle without virtual mass | 0.0565 | kg | $\pm 0.005$ |
| $\frac{m_{ex}}{m_b+m_g}$ | Horizontal virtual mass ratio | 1.4 | | $\pm 0.2$ |
| $\frac{m_{ez}}{m_b+m_g}$ | Vertical virtual mass ratio | 2.1 | | $\pm 0.4$ |
| $I_{ez}$ | Experimental inertia around the $z$ axis | $2.7 * 10^{-3}$ | $\text{kg} \cdot \text{m}^2$ | $\pm 0.2 * 10^{-3}$ |
| $I_{ex}$ | Experimental inertia around the $x$ and the $y$ axis | $6.0 * 10^{-3}$ | $\text{kg} \cdot \text{m}^2$ | $\pm 10^{-3}$ |
| $C_{rz}$ | Rotational drag coefficient about $z$ | $2.7 * 10^{-4}$ | | $\pm 0.7 * 10^{-4}$ |
| $C_{rx}$ | Rotational drag coefficient about $x$ | $9.7 * 10^{-4}$ | | $\pm 2 * 10^{-4}$ |

## 5. THE GENERAL OPTIMAL CONTROL PROBLEM

Mathematically, the general optimal control problem is defined as follows: given the state trajectories $\mathbf{s}(t)$, $t \subset [t_0, t_f]$, and times $t_o, t_f$, find the optimal control inputs $\mathbf{u}(t)$, $t \subset [t_0, t_f]$, to minimize the following performance index:

$$J = \phi(\mathbf{s}(t_0), \mathbf{s}(t_f), t_0, t_f) + \int_{t_o}^{t_f} L(\mathbf{s}(t), \mathbf{u}(t), t) dt \tag{17}$$

subject to the differential constraints

$$\dot{\mathbf{s}}(t) = f(\mathbf{s}(t), \mathbf{u}(t), t), t \subset [t_o, t_f] \tag{18}$$

the path constraints

$$h_l \leq h(\mathbf{s}(t), \mathbf{u}(t), t) \leq h_u, t \subset [t_o, t_f] \tag{19}$$

the events

$$e_l \leq e(\mathbf{s}(t_o), \mathbf{u}(t_o), \mathbf{s}(t_f), \mathbf{u}(t_f), t_o, t_f) \leq e_u, t \subset [t_o, t_f] \tag{20}$$

the bound constraints

$$\begin{gathered} \mathbf{u}_l \leq \mathbf{u}(t) \leq \mathbf{u}_u, t \subset [t_o, t_f] \quad \mathbf{s}_l \leq \mathbf{s}(t) \leq \mathbf{s}_u, t \subset [t_o, t_f] \\ t_{fL} \leq t_f \leq t_{fU} \quad t_{0L} \leq t_0 \leq t_{0U} \end{gathered} \tag{21}$$

and the constraint $t_f - t_o \geq 0$. The path constraint $h$ can include obstacles, expressed as restrictions on the positions $x(t)$, $y(t)$ and $z(t)$, where the subscripts $u$ and $l$ are for upper and lower limits. For example, the constraint $x^2(t) + y^2(t) \geq 1$ would exclude all paths going through a circle of radius one centred at the origin. The event constraint $e$ is used to specify a range for the start and end point of the time, the states and the control inputs of the problem.

The problem can also be described in multiple phases, which is useful when discontinuities appear in the problem or when the equations governing the system change (for example in the case of payload deliveries). In this case, additional events would usually be added to link the phases as described in the general formulation of the optimal control problem [11].

The optimal control problem was solved using a pseudo-spectral solver. With this method, the states and the control inputs are represented with orthogonal functions. In this paper, Legendre polynomials are

Table 2. Position and velocity conditions for the first simulation.

| Time | $x_x^i$ (m) | $x_y^i$ (m) | $x_z^i$ (m) | $\phi$ (rad) | $\theta$ (rad) | $\psi$ (rad) |
|---|---|---|---|---|---|---|
| Initial | 0 | 0 | 0 | 0 | 0 | 0 |
| Final | 1.5 | 0.5 | 0 | 0 | 0 | 1 |
| | $\dot{x}_x^b$ (m/s) | $\dot{x}_y^b$ (m/s) | $\dot{x}_z^b$ (m/s) | $p$ (rad/s) | $q$ (rad/s) | $r$ (rad/s) |
| Initial | 0 | 0 | 0 | 0 | 0 | 0 |
| Final | 0 | 0 | 0 | 0 | 0 | 0 |

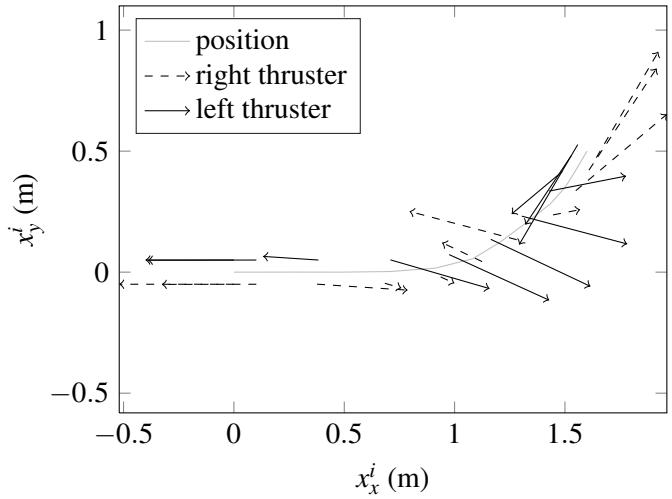


Fig. 3. First solution path and normalized thrust of the right (dashed) and left (solid) motors at select positions.

used since they can be differentiated and integrated very quickly [11]. The optimal control problem is then transformed into a non-linear programming problem, where the function to optimize while respecting the differential constraints is the Lagrangian $L$. For the trajectory problem studied in this paper, the Lagrangian is the flight time $L = t_f$, and the constraints to be respected are the differential constraints of motion. The search space is limited by the physical bounds of the experimental area and the limits of the vehicle including: the maximum thrust, speed and angular speed of the vehicle. The advantages of the pseudo-spectral approach are that the convergence is exponential and the results follow closely the dynamic model.

The pseudo-spectral solver was implemented in the PSOPT open source optimal control software package, the complete description of which is given in [11].

## 6. SIMULATION RESULTS

Two simulated problems are presented to illustrate the trajectory generation using optimal control.

### 6.1. First Simulation

The first problem requires the vehicle to move forward and to the left at an angle and arrive at the desired coordinates with zero final velocity. The numerical values of the initial and final conditions used by the solver are listed in Table 2. Although the full vehicle dynamics are solved in the simulations, only the planar motion is shown in Fig. 3, along with the normalized thrust for each motor at constant time intervals along the trajectory. In the complete solutions, the thrust from the left and right propellers creates a torque which modifies the pitch and, consequently, changes the altitude of the vehicle. Maintaining the desired altitude would require an additional thruster aligned with the vertical axis of the vehicle.

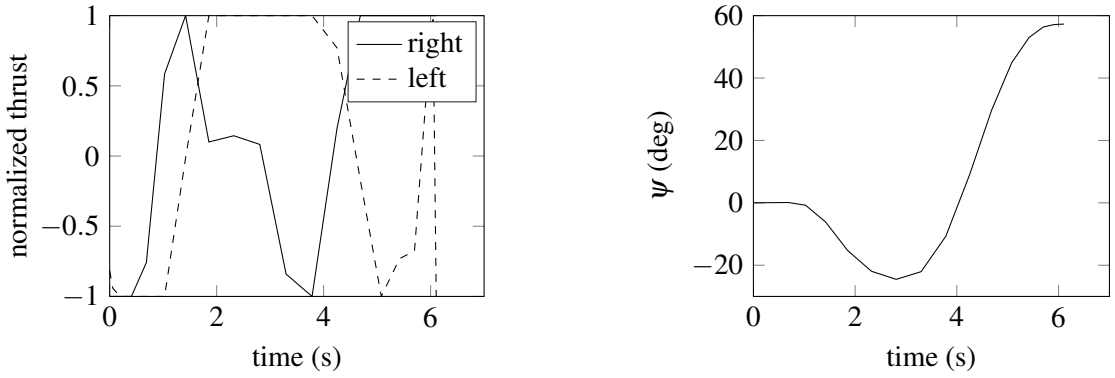


(a) Normalized thrust

(b) Yaw orientation

Fig. 4. First simulation thrust and yaw angle.

Table 3. Simulation parameters for the second experiment.

| Time | $x_x^i$ (m) | $x_y^i$ (m) | $x_z^i$ (m) | $\phi$ (rad) | $\theta$ (rad) | $\psi$ (rad) |
|---|---|---|---|---|---|---|
| Initial | 0 | 0 | 0 | 0 | 0 | 0 |
| Final | 0 | 0.3 | 0 | 0 | 0 | 0 |
| | $\dot{x}_x^b$ (m/s) | $\dot{x}_y^b$ (m/s) | $\dot{x}_z^b$ (m/s) | $p$ (rad/s) | $q$ (rad/s) | $r$ (rad/s) |
| Initial | 0 | 0 | 0 | 0 | 0 | 0 |
| Final | 0 | 0.1 | 0 | 0 | 0 | 0 |

From Fig. 3, the vehicle accelerates in a straight line in the first second of the trajectory. Then, the vehicle points outwards of the path and reverses its thrust to reorient the vehicle's velocity vector toward the final position. This is further illustrated in the thrust plot in Fig. 4a, and in Fig. 4b. In the final section of the path, the vehicle travels in a straight line, accelerating and then decelerating to reach the desired position, orientation, and velocity.

### 6.2. Second Simulation

The second simulation demonstrates how lateral movements are possible with the airship, even though there are no thrusters capable of directly producing a lateral force. The airship is required to move directly to the left of the starting point and arrive at the desired coordinates at the same orientation, but with a lateral speed. This kind of manoeuvrer could be useful for storing the airship in a similar manner to parallel parking for cars. Due to the lateral movement, the path would be impossible to generate with a traditional linear controller.

The initial and final conditions for the second problem are presented in Table 3 and the trajectory generated is shown in Fig. 5. The commands sent to the motor are shown in Fig. 6a and the yaw orientation of the vehicle as a function of time is shown in Fig. 6b.

At the beginning of the manoeuvrer, the vehicle accelerates and turns to the right by reversing the right thruster. This induces lateral velocity in the vehicle. In the final section of the path, the motion in the $x$ direction is halted, and the vehicle is reoriented by reversing both thrusters while maintaining the induced velocity in the $y$ direction.

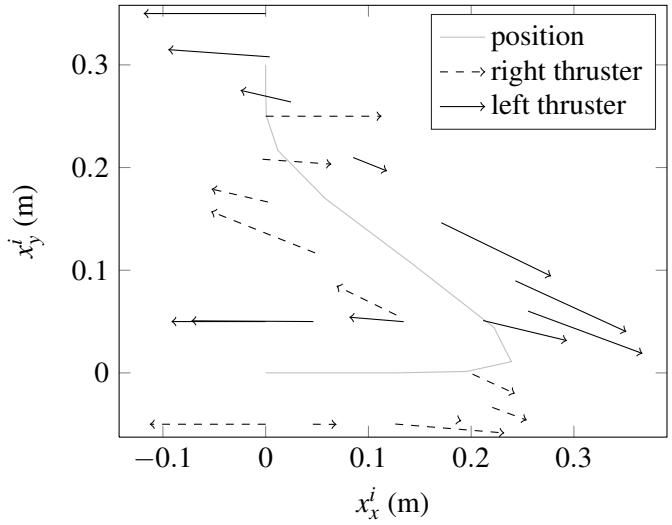


Fig. 5. Second solution path and normalized thrust of the right (dashed) and left (solid) motors at select positions.

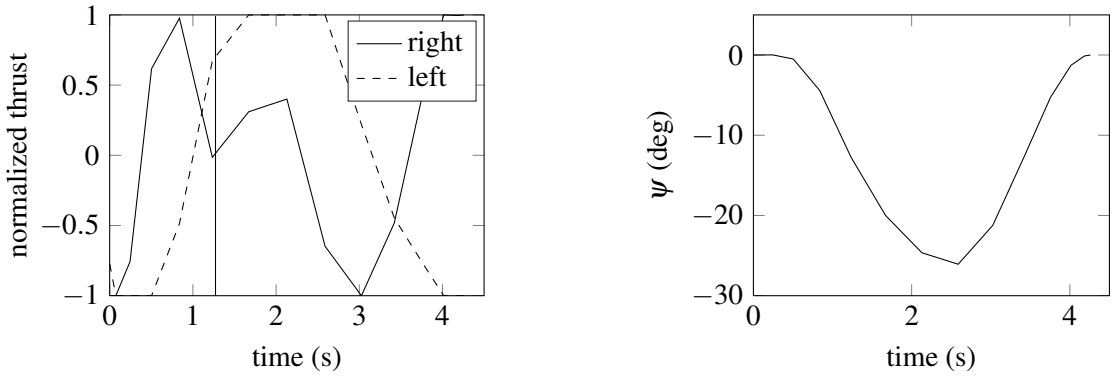


(a) Normalized thrust

(b) Yaw orientation

Fig. 6. Thrust and yaw angle as a function of time for the second experiment.

## 7. DISCUSSION

The optimal solver is used to generate very complex paths while respecting the differential equations of the dynamic model. The time to solve the trajectory planning problems was between 1 and 30 seconds on a modern computer. An important advantage of the optimal solver is the flexibility of the mathematical formulation, as almost any dynamic systems can be used. For instance, a propeller model taking into account the inertia and the drag of the propeller could be added to the optimal control problem without changing the formulation. The limitations of the solver include convergence, the need for an initial guess, and the presence of discontinuities in the polynomials used to represent the states. In the first case, the convergence of the solution is dependent on the initial guess. If the initial guess is poor or, alternatively, if the search space is large, the solver can have difficulties converging to a solution. In the simulations presented in this paper, a linear interpolation between the initial and final condition was used as an initial guess for every state, and the controls were initially assumed to be zero. In certain cases where the solution diverged significantly from the initial guess, the solver would fail to converge. In the second case, discontinuities in the polynomials representing the states were approximated with large errors. This can be seen in Fig. 6 at 1.25 s when the

vehicle reverses thrust. This issue can be resolved by decomposing the problem into multiple phases as noted in Section 5.

The quality of the resulting trajectory is also highly dependent on the precision and accuracy of the model. Naturally, drift will occur as the vehicle travels along the path as a result of small errors in the models and changing environmental conditions. Therefore a feedback controller would still be required. Alternatively, it would also be possible to re-plan the path using the optimal solver after at certain error threshold is reached, and the dynamic model could be updated to better reflect changes in model and environmental conditions.

Given the strengths and limitations of the optimal solver, the results could be used in real applications to pre-calculate specific open-loop manoeuvres. For instance, parts of the landing and take-off procedure of a small airship could be open-loop, and the optimal solver could be used to generate the commands. Other applications include rapid reorientation manoeuvres for obstacle avoidance.

## 8. CONCLUSIONS

This research described the theoretical and experimental modelling of a small airship. The optimal trajectory problem was formulated as an optimal control problem and solved using a pseudo-spectral method. The results demonstrated that complex and locally optimal trajectories could be generated for short duration manoeuvres.

## REFERENCES


1. Waishek, J., Dogan, A. and Bestaoui, Y., "Investigation into the time varying mass effect on airship dynamics response", in *Proceedings 47th AIAA Aerospace Sciences Meeting Including The New Horizons Forum and Aerospace Exposition*, January, 2009.
2. Cummings, J.S., "Long Endurance Multi-Intelligence Vehicle (LEMV) Agreement Signed", 2010.
3. Wang, H., Li, Q. and Cheng, N., "Real-time path planning for low altitude flight based on A* algorithm and TF/TA algorithm", in *Proceedings Automation Science and Engineering (CASE)*, pp. 837–842, 2012.
4. Meng, B.b. and Gao, X., "UAV path planning based on bidirectional sparse A* search algorithm", in *Proceedings Intelligent Computation Technology and Automation*, pp. 1106–1109, 2010.
5. Casalino, L., Colasurdo, G. and Pastrone, D., "Optimal low-thrust escape trajectories using gravity assist", *Journal of Guidance, Control, and Dynamics*, Vol. 22, No. 5, pp. 637–642, 1999.
6. Zhuang, Y., Ma, G., Huang, H. and Li, C., "Real-time trajectory optimization of an underactuated rigid spacecraft using differential flatness", *Aerospace Science and Technology*, Vol. 23, No. 1, pp. 132–139, 2012.
7. Sorensen, J.A., Morello, S.A. and Erzberger, H., "Application of trajectory optimization principles to minimize aircraft operating costs", in *Proceedings 18th IEEE Conference on Decision and Control including the Symposium on Adaptive Processes*, Vol. 18, pp. 415–421, 1979.
8. Legras, B. and Dritschel, D.G., "A comparison of the contour surgery and pseudo-spectral methods", *Journal of Computational Physics*, Vol. 104, No. 2, pp. 287–302, 1993.
9. Hygounenc, E., Jung, I.K., Souères, P. and Lacroix, S., "The autonomous blimp project of LAAS-CNRS: Achievements in flight control and terrain mapping", *The International Journal of Robotics Research*, Vol. 23, pp. 473–511, 2004.
10. Li, Y., Nahon, M. and Sharf, I., "Airship dynamics modeling: A literature review", *Progress in Aerospace Sciences*, Vol. 47, No. 3, pp. 217–239, April 2011.
11. Becerra, V.M., *PSOPT optimal control solver user manual (Release 3)*, 2011.